14th IAPR International Conference on Machine Vision Applications (MVA)
May 18-22, 2015. Miraikan, Tokyo, Japan

3D lung nodule candidate detection in multiple scales

Jorge Novo, Luis Gonçalves, Ana Maria Mendonça, Aurélio Campilho
INESC TEC and Faculty of Engineering, University of Porto
FEUP Campus, Dr. Roberto Frias 4200 - 465 Porto (Portugal)

Abstract

Lung cancer is mainly diagnosed by the identification of malignant nodules in the lung parenchyma. For that purpose, the identification of all the possible structures that could be suspicious of lung nodules became a crucial task in any lung cancer computer aided diagnosis (CAD) system.

In this paper, a new approach for lung nodule candidate identification is proposed. This method uses a 3D medialness Hessian-based filtering to identify round shape structures that could be identified as nodules. This technique, that demonstrated its accuracy in lung vesselness extraction, provides clearer candidates than other approaches, providing less response in the presence of noise artifacts and returns a better continuity in vessels, mostly responsible for false positives. That way, they will be better distinguishable from the nodules in posterior analysis.

This approach was validated in 120 scans from the LIDC/IDRI image database. They include 212 nodules with diameters in the range 3 mm to 30 mm. The results demonstrate that our approach is capable of identifying most of the nodules and include less false positives than other approaches, facilitating a posterior task for false positive removal.

1 Introduction and previous work

Nowadays, from all the cancers, lung cancer is the most dangerous and main cause of death. As reference, the American Cancer Society estimated, for 2014, that lung cancer represents approximately 27% of all cancer deaths [1]. That makes the early detection and diagnosis a crucial task to maximize the chances of survival.

There are different approaches that face this problem. All the methods try to identify malignant lung nodules, as in chest radiography [2]. However, from all of them, the analysis in chest Computed Tomography (CT) is one of the most employed, providing better information for the detection of malignant nodules.

Lung cancer diagnosis methodologies can be generally organized in 5 different steps: lung parenchyma extraction, nodule candidates identification, nodule detection, benign/malignant differentiation and, therefore, the final lung cancer diagnosis. Lung parenchyma extraction involves the segmentation of lung region. In our case, we used region growing to obtain the ROI, remove the traquea and refine the contour to include all possible juxtapleural nodules, as Novo *et al.* [3] proposed.

The next step is the lung nodule detection. Many of the proposed CAD systems have two phases: first, the identification of all structures that could be nodules; second, the false positive (FP) reduction. Generally, nodules present a round shape with a blob-like structure but presenting a large variability in terms of size, shape or irregular contours and the possibility of nodules attached to vessels or lungs walls. All of this imply that nodule candidate detectors have to be flexible enough to include all existing nodules, but restrictive enough to avoid as much FP structures as possible. This is where this paper is placed, in particular, in the nodule candidate detector.

Over the years, a large amount of techniques to face this problem were published. Some authors performed different image transformations in order to enhance the nodules from other structures and separate them by thresholding [4]. Others, employed several different gray-level techniques in order to obtain the final candidates [5, 6]. Other approaches used cylindrical and spherical filters to recover the structures with potential of being nodules [7, 8], idea that was also used in [9], identifying circular and semicircular (juxtapleural and attached nodules) by template matching.

Our focus is one of the most relevant and referenced works, proposed by Murphy *et al.* [10]. This method calculated the Curvedness (CV) and Shape Index (SI), two local image features, that are thresholded to define the nodule candidates.

In this paper, we use the structural information of the Hessian matrix to identify the nodule candidates. However, we used the principle of central adaptive medialness (instead of CV and SI) that was proposed by [11] for the detection of tubular structures in 3D imaging. This method was recently applied to lung vessel extraction demonstrating its accurate response as it was the winner of the VESSEL12 challenge [12], vessel segmentation in lung CT scans. This approach offers better coherence in vessel detection and connectivity and is more robust with respect to noise, desirable properties for lung nodule detection.

2 Methodology

Our approach uses an image enhancement filter that employs the eigenvalues derived from the 3D Hessian matrix at each voxel to identify those regions in the image with round structures. Given the large nodule size variability we use a multi-scale method, based on the Gaussian second order derivative of an image I with scale σ at a voxel x, given by:

$$\frac{\partial^2 I_\sigma}{\partial x^2} = I(x) * \frac{\partial^2 G(\sigma, x)}{\partial x^2} \quad (1)$$

Based on (1) we compute the 3×3 Hessian matrix, at the voxel $x = (x_1, x_2, x_3)$ for a given σ and derives the eigenvalues $|\lambda_1| \leq |\lambda_2| \leq |\lambda_3|$. Using the λ's, different enhancement methods can be applied with the idea of filtering those structures to be considered as nodule candidates. Thus, for a given σ, we calculate $V_\sigma(x)$ as the response of a given enhancement method in a voxel x.

The final response is calculated as the maximum response at each voxel x over the range of σ's:

$$V(x) = \max_{\sigma_1 \leq \sigma_j \leq \sigma_n} V_{\sigma_j}(x) \quad (2)$$

Below, we describe the enhancement approaches ($V_\sigma(x)$) included in this paper, that is, using SI and CV, as defined in [10], and our proposed approach that uses the central adaptive medialness as in [11].

2.1 Shape Index and Curvedness approach

In [10], the authors down-sample the image and apply a Gaussian filter ($\sigma = 1$) to reduce the noise influence. After obtaining the principal curvatures with $\sigma = 1$, the authors derive the SI and CV as:

$$SI = \frac{2}{\pi} arctan\left(\frac{\lambda_1+\lambda_2}{\lambda_1-\lambda_2}\right) \quad CV = \sqrt{\lambda_1^2+\lambda_2^2} \quad (3)$$

Finally, hysteresis thresholding is used to find the candidates. This method also defined a more relaxed level for juxtapleural nodules, in order to preserve them.

In our implementation, we calculate the eigenvalues over a range of σ's (instead a fixed one as used in [10]).

2.2 Central adaptive medialness approach

We use the central adaptive medialness principle [11] that was firstly defined to detect $3D$ tubular structures and recently applied for lung vessel extraction.

This method uses λ_1, λ_2 and λ_3 as follows:

$$V(\sigma, x) = \begin{cases} 0 & \lambda_1 + \lambda_2 + \lambda_3 \geq 0 \\ -\frac{\lambda_2}{\lambda_3} \cdot (\lambda_2 + \lambda_3) & \text{otherwise} \end{cases} \quad (4)$$

Basically, this method is only applied where the sum of the eigenvalues is less than 0, that is, for bright objects. In this case, we use the two largest eigenvalues to measure the structure strength, and their ratio is applied to correct deviation from the center of the detected structure.

As main advantages, this approach offers higher robustness as it does not require any Gaussian smoothing, being more sensitive to small nodules.

Most of the FPs are due to all the bronchi and vessels in the image. This method offers a better continuity in vasculature implying less identification of FPs and also facilitating *a posteriori* analysis distinguishing the bronchi and vessels (tubular-like structures) from nodules (blob-like structures).

2.3 Final lung nodule candidates refinement

Once the thresholded candidate image is obtained, the final nodule is obtained by grouping the bright pixels in clusters by connectivity. Then, it clears the image with tiny candidates (mainly derived from noisy artifacts). The remaining candidates are grouped in 3 different types, according to their size:

Small candidates: candidates with small number of pixels are grown, for making possible a more reliable characterization.

Intermediate candidates: candidates that are directly taken to the final results.

Large Candidates: we assume that these candidates are juxtavascular nodules (nodules attached to vessels). In this case, we apply a progressive erode until complete vessel removal. In each eroding step, we take all the small broken parts as new candidates. In particular, we dilate with the same structure element in the erosion and mask the result with the original candidates image. Figure 1 shows examples of small and juxtavascular nodule detection.

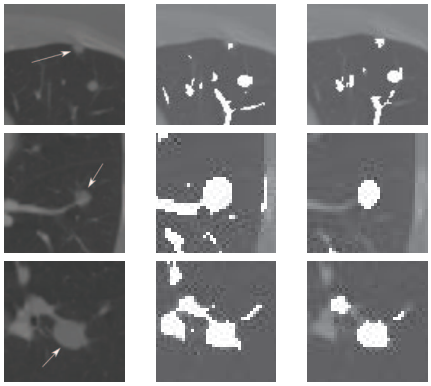

(a) (b) (c)

Figure 1. Examples of final candidate refinement. 1^{st} row, growing of a small nodule candidate. 2^{nd} and 3^{rd} rows, separation of juxtavascular nodules. (a) Original image. (b) Candidates before refinement. (c) Final candidates detection.

(a) (b) (c)

Figure 2. Example of nodule candidate detection. (a) Original image. (b) Candidates after initial detection. (c) Final detected candidates.

As in the dilation process new small structures could be added, we apply an additional cleaning step, but, as they are the final candidates, with higher thresholds. Figure 2 shows an example of candidate detection including initial detection after applying the central adaptive medialness criterion and the result after the final refinement of the candidates.

2.4 Candidate features and classifiers

To reduce the number of FPs we characterize the nodule candidates with a set of features that are used in a classification step. A small set of basic features and a set of basic classifiers were employed to evaluate the generated candidates. Regarding the features, some of them are inspired in the first set proposed by Murphy *et al* [10]. The measurements are calculated in millimeters. These features are:

- **Cluster size**, number of voxels.
- **Compactness1** $= \frac{ClusterSize}{(dim_x)\cdot(dim_y)\cdot(dim_z)}$.
- **Compactness2** $= \frac{ClusterSize}{(max\_dim^3)}$.
- **Ratio1** $= \frac{max\_dim}{min\_dim}$. **Ratio2**, $\frac{max\_dim}{med\_dim}$.
- **RatioEi1** $= \frac{\lambda_2}{\lambda_3}$ **RatioEi2** $= \frac{\lambda_1}{\lambda_3}$ **RatioEi3** $= \frac{\lambda_1}{\lambda_2}$
- **RatioEi4** = ratioEi1 · ratioEi2 · ratioEi3.

Given a *sphere_S*, a sphere at the candidate location with radius the mean of the dimensions:

Table 1. Threshold for SI and CV.

	Initial seed thresholds		Hysteresis thresholds	
	Shape Index	Curvedness	Shape Index	Curvedness
	0.5	0.01	0.45	0.08
Pleural	0.4	0.005	0.35	0.003

- **Sphericity1**, $\frac{num\_cluster\_voxels\_in\_sphere\_S}{num\_voxels\_sphere\_S}$.
- **Sphericity2**, $\frac{num\_cluster\_voxels\_in\_sphere\_S}{num\_voxels\_nodule}$.
- **intensity_max, intensity_min, intensity_mean, intensity_median and intensity_std** are the maximum, minimum, mean, median and standard deviation of the cluster.

Sequential Forward Feature Selection (SFFS), with inter-intra criterion as the evaluation measure was used. It was selected as it is fast to compute, which is ideal for a large amount of data. For classification, different classifiers were used, the Linear Discriminant classifier, the Quadratic Discriminant classifier and Parzen classifier. The system was evaluated using sensitivity.

3 Results

3.1 Lung image database

We tested the methodology on 120 different chest CT scans from the LIDC-IDRI image database [13], with a variable number of 512×512 slices, between 102 and 310, with image intensities in the range $[0 - 1]$. These scans contain 212 nodules identified by up to 4 radiologists. Each radiologist manually segmented each identified nodule. This 3D segmentation is used as groundtruth to identify candidates that belong to nodules. The scans were taken from a heterogeneous range of scanner models and technical acquisition parameters.

Only solid and part-solid nodules were considered. No other restriction was introduced to include the lung nodules, as defined by the LIDC-IDRI database, in terms of: subtlety, internal structure, calcification, sphericity, margin, lobulation, spiculation, texture and malignancy. A large variability of nodules in terms of size and characteristics is represented. Finally, for efficiency, the images were down-sampled to 256×256.

3.2 Parameter tuning

Given the large nodule variability and image conditions, the parameters used were set flexible enough to be able to detect most of them.

For SI and CV computation, we used a range of σ's between 0.5 and 3.5, increasing 0.5 steps. As explained before, the resultant eigenvalues of each combination were taken to calculate the SI and CV parameters. The final parameters at each voxel were taken as the maximum value among scales. Finally, Table 1 shows the SI and CV thresholds used to obtain the candidate image.

Our approach was directly applied, without any preprocessing. To the result image, it is applied a threshold of 0.08 to obtain the candidates and a lower threshold of 0.001 for small candidates.

In the candidate refinement phase, only nodules with sizes between 10 and 500 voxels. Moreover, the initial and final candidates cleaning establish as minimum sizes 2 and 5 voxels for juxtapleural candidates, and 5 and 10 voxels for candidates for the rest of the candidates.

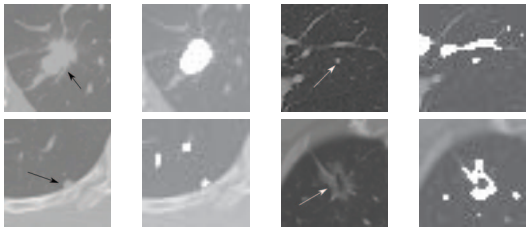

(a) (b) (c) (d)

Figure 3. Examples of detected nodules. (a)(c) Input images. (b)(d) Nodule candidates.

Table 2. Results after lung candidates detection.

Methodology	Sensitivity after processing	FP per scan
Murphy *et al.*	96.22%	881
Proposed	98.11%	397

3.3 Analysis of the results

Firstly, a nodule is considered successfully detected if there is any candidate that overlaps with the ground truth provided by the specialists. As shown in Table 2, the candidate detection with both methodologies has a good sensitivity, even better with the proposed approach. The few missed positive cases are extremely complicated ones. They belong to small juxtavascular nodules that are placed in the continuity of a vessel. They were initially detected but removed in the eroding process.

Figure 3 shows examples representing the large nodule variability. In particular, the first row presents two different nodules in terms of size, a big nodule and a small nodule. The second row presents two complicated detections in terms of shape and position, a small juxtapleural nodule and a complex part solid nodule.

Table 2 shows the results for the candidate identification. The central adaptive medialness approach, as explained before, offers a good response in the nodules as well as it includes significantly less FPs. Moreover, as the proposed approach offers a better continuity in the vessels, responsible for many of the FPs, the method generates less juxtavascular FPs.

Additionally, we tested the potential of the method in reducing the number of FPs by introducing an additional classification step using the set of nodule features mentioned before. For that purpose we varied the number of features between 5 and 10. SFFS selected mainly shape and morphology features, as most of the FPs have a non-blob structure. Intensity based features are always selected after the 5^{th} place. That happens due to the large variability in image conditions arising from different machines, configurations, etc. Moreover, we include a large variability of nodules. As result, the global intensity measures are not homogeneous, penalizing their discrimination relevance.

Table 3 shows the performance results evaluated using sensitivity and FP removal for both approaches. The proposed approach generates a low number of FP candidates. Overall, it reduces significantly the number of FPs, concluding with a considerably lower set comparing with the approach without the classification step. The results were obtained with the classifier that offered the best results. In this case, they were

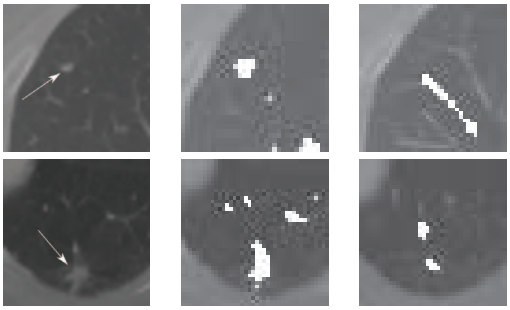

Figure 4. Examples of missed nodules after classification due to part of vessels attached. Original image, candidate in the given slice and continuity of the nodule candidate along adjacent vessel in consecutive slice, respectively.

obtained by the LDC.

Regarding the sensitivity reduction, almost all of the missed nodule candidates are juxtavascular nodules. In this case, the refinement process sometimes includes small parts of vessels that remain attached to the candidate. That way, these candidates have a not so similar blob shape, as seen in Figure 4. As the classification step uses mainly shape and morphological features, these candidates can be easily mistaken as FP candidates, as they do not resemble blob like structures.

In terms of efficiency, both methods uses the same structure, produces the initial candidates derived from the enhancement filtering using the eigenvalues and then, apply a sequence of operations to refine the final nodule candidates. For that reason, the computational cost of the methods depends directly on the number of this initial set of identified FPs. As the proposed method produces significantly less initial FPs, the rest of the method is significantly faster with respect to the Murphy's approach. Using a specific patient, the candidate identification (before classification) using the Murphy's method, and a final set of 341 candidates took close to 6 minutes to be obtained. The same process with the proposed method took 3.5 minutes with a final set of 121 candidates.

4 Conclusions

In this paper, a new methodology for chest CT lung nodule candidate selection is proposed. The method uses the principle of central adaptive medialness [11] for the identification of all the structures that could be lung nodules. This approach offers a better response to noise and vessels than other Hessian based approaches in reducing the FP rate per scan. The method was tested on 120 scans including 212 nodules with solid/part-solid texture, detecting most of them.

We also tested the candidates with a small set of features and basic classifiers. As the experiments show, this new approach can reduce the FPs significantly. The method provides an accurate detection in the largely variable set of nodules. All the initial non detected nodules and most of the miss-classifications come from juxtavascular nodules that, in the refinement process, are removed or they still have attached vessel parts. In future work, we plan to perform a more accurate extraction of juxtavascular nodules. Moreover, a more advanced feature extraction and classification process will be developed in order to improve the performance of the method.

Table 3. Results after FP reduction.

Methodology	Sensitivity	Final FP/scan
Murphy *et al.*	89.71%	221
Proposed	88.65%	107

4.1 Acknowledgments

This work is financed by the FCT - Fundação para a Ciência e a Tecnologia (Portuguese Foundation for Science and Technology) within project UID/EEA/50014/2013 and the SFRH/BPD/85663/2012 grant contract.

References

[1] American Cancer Society: "Cancer Facts and Figures", 2014.

[2] C.S. Pereira, H. Fernandes *et al.*: "Detection of lung nodule candidates in chest radiographs", *IbPRIA'07*, 4478, 170–177, 2007.

[3] J. Novo, J. Rouco *et al.*: "Reliable Lung Segmentation Methodology by Including Juxtapleural Nodules", *ICIAR'14*, 8815, 227–235, 2014.

[4] H. Arimura, S. Katsuragawa *et al.*: "Computerized scheme for automated detection of lung nodules in low-dose computed tomography images for lung cancer screening", *Academic Radiology*, 11, 617–629, 2004.

[5] J. P. Ko, M. Betke: "Chest CT: automated nodule detection and assessment of change over time–preliminary experience", *Radiology*, 218, 267–273, 2001.

[6] B. Zhao, M. S. Ginsberg *et al.*: "Application of the LDM algorithm to identify small lung nodules on low-dose MSCT scans", *Medical Imaging 2004: Imaging Processing*, 818–823, 2004.

[7] H. Takizawa, K. Shigemoto *et al.*: "A recognition method of lung nodule shadows in X-Ray CT images using 3D object models", *Journal Image and Graphics*, 3, 533–545, 2003.

[8] D. Paik, C. Beaulieu *et al.*: "Surface normal overlap: a computer-aided detection algorithm with application to colonic polyps and lung nodules in helical CT", *IEEE Trans. on Med. Imaging*, 23, 661–675, 2004.

[9] Y. Lee, T. Hara *et al.*: "Automated detection of pulmonary nodules in helical CT images based on an improved template-matching technique", *IEEE Trans. on Med. Imaging*, 20, 595–604, 2001.

[10] K. Murphy, B. van Ginneken *et al.*: "A large-scale evaluation of automatic pulmonary nodule detection in chest CT using local image features and k-nearest-neighbour classification", *Medical Image Analysis*, 13, 757–770, 2009.

[11] K. Krissian, G. Malandain *et al.*: "Model based detection of tubular structures in 3d images", *Computer Vision and Image Understanding*, 80, 130–171, 2000.

[12] R.D. Rudyanto, S. Kerkstra *et al.*: "Comparing algorithms for automated vessel segmentation in computed tomography scans of the lung: the VESSEL12 study", *Medical Image Analysis*, 18, 1217–1232, 2014.

[13] S.G. Armato, G. McLennan *et al.*: "The lung image database consortium (LIDC) and image database resource initiative (IDRI): a completed reference database of lung nodules on CT scans", *Medical Physics*, 38, 915–931, 2011.